Cell Reports, Volume *23*

Supplemental Information

NMDA Receptor Autoantibodies in Autoimmune Encephalitis Cause a Subunit-Specific Nanoscale Redistribution of NMDA Receptors

Laurent Ladépêche, Jesús Planagumà, Shreyasi Thakur, Irina Suárez, Makoto Hara, Joseph Steven Borbely, Angel Sandoval, Lara Laparra-Cuervo, Josep Dalmau, and Melike Lakadamyali

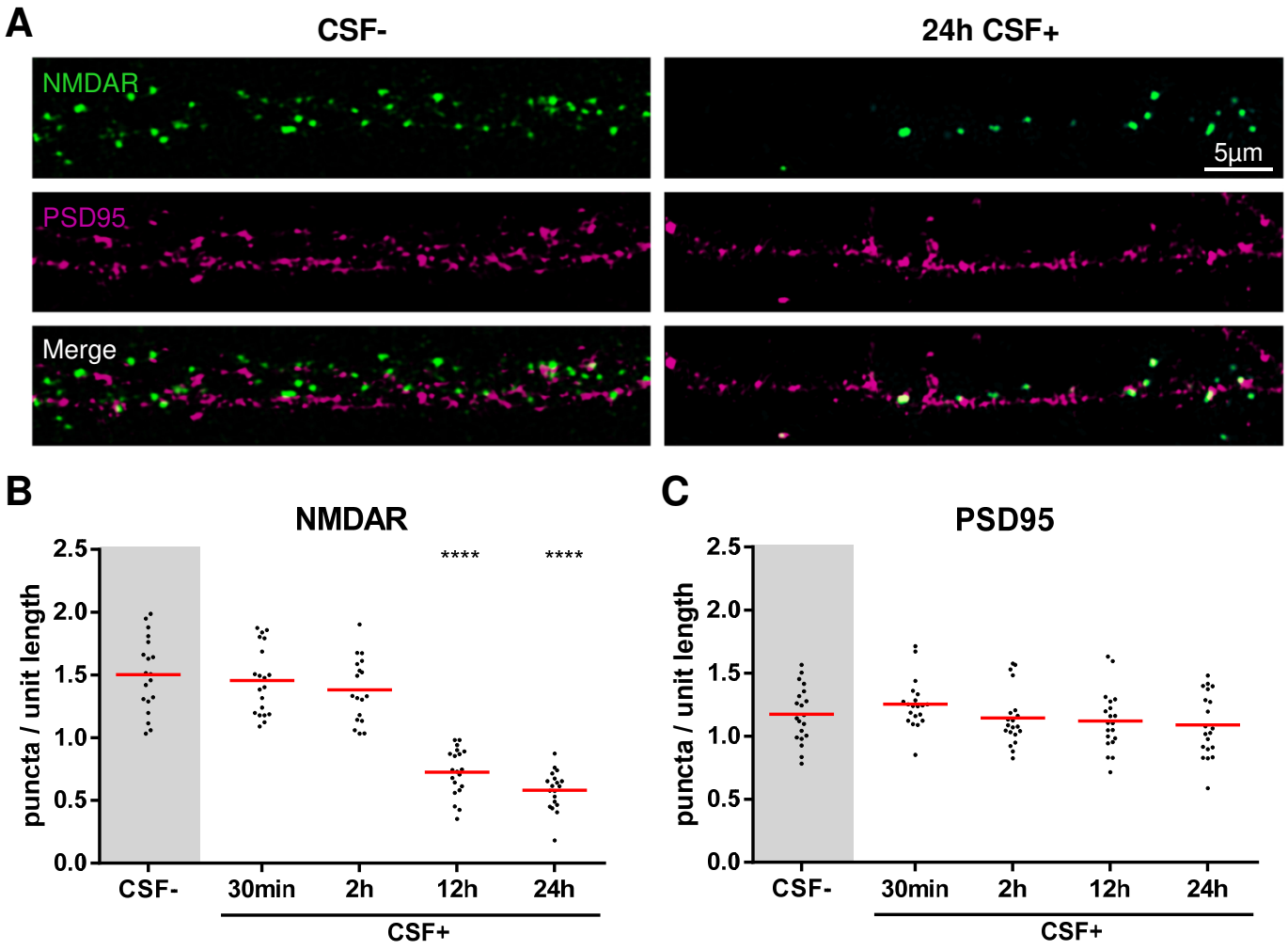

Figure S1: NMDAR autoantibodies induce a reduction in the surface density of NMDAR (related to Figure 1)

(**A**) Representative confocal images of surface NMDAR (green, upper panels) labelled together with PSD95 (magenta, middle panels) after 24 hr of incubation with control or patients' CSF (CSF-, upper panels, and CSF+, lower panels, respectively).

(**B-C**) Neurons were treated for 30 min, 2, 6, 12 or 24 hr with control or patients' CSF (CSF- and CSF+ respectively) and the number of NMDAR puncta per unit length (µm) of dendrite was measured for surface NMDAR (**B**) and PSD95 (**C**). Red lines represent means and the dots correspond to individual cells (NMDAR n = 19, 20, 18, 20 and 19 fields of view respectively, from left to right; NMDAR n = 20, 20, 20, 20 and 20 fields of view respectively, from left to right; ****$p < 0.0001$, Kruskal-Wallis test).

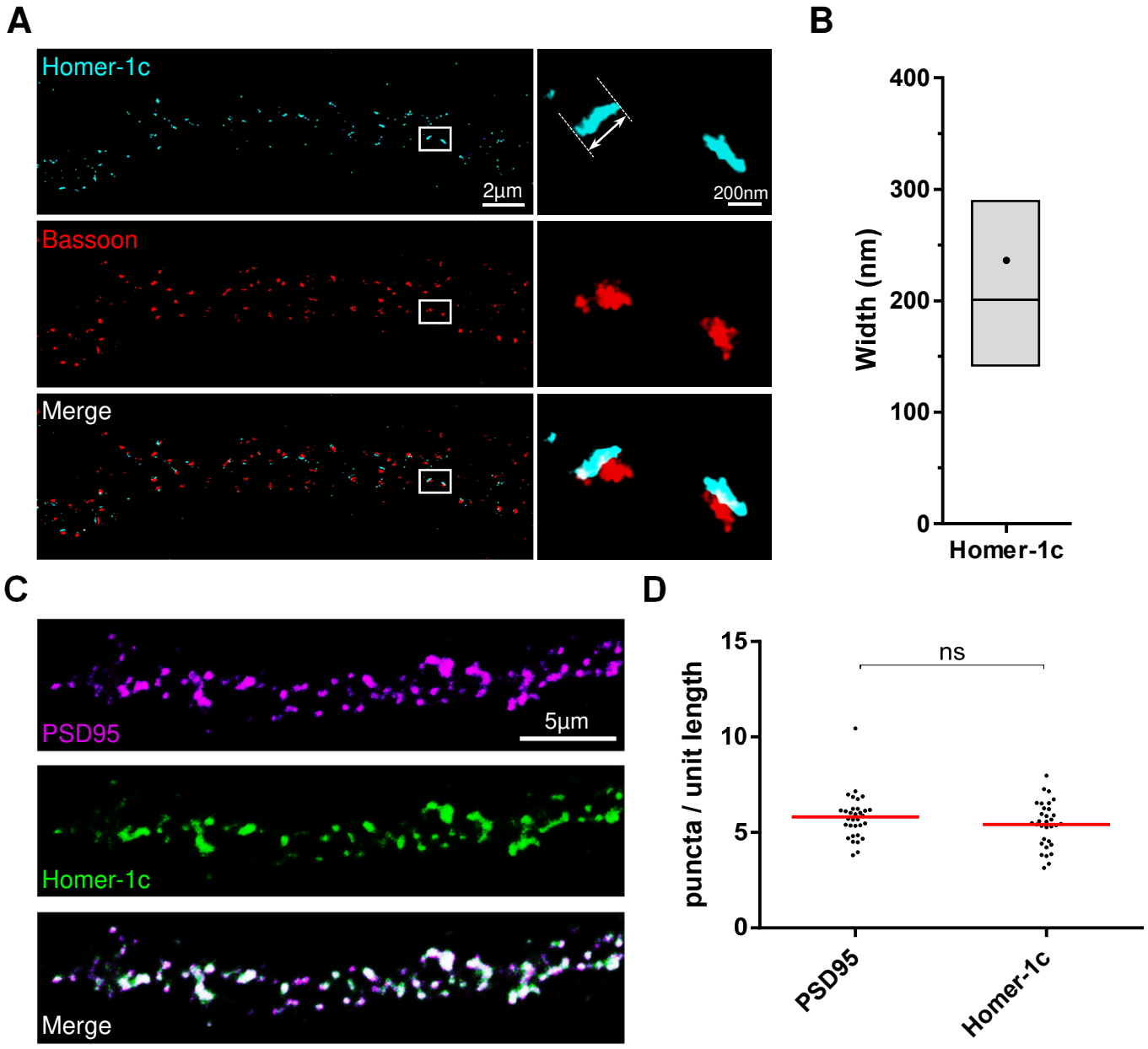

Figure S2: Imaging of the postsynaptic density protein Homer-1c as a synaptic structural reference (related to Figure 1)

(**A**) A representative STORM image of the postsynaptic protein Homer-1c (cyan, upper panels), and the presynaptic protein Bassoon (red, middle panels) allowed visualization of the synaptic complex (merge, lower panels).

(**B**) Quantification of the width of the Homer-1c as indicated by the dashed lines and arrows in A (upper panels, zoom). The box, line and dot correspond to interquartile range (IQR, 25th-75th percentile), median and mean, respectively (n = 622 synapses).

(**C**) Representative confocal images of the postsynaptic proteins PSD95 (magenta, upper panel) and Homer-1c (green, middle panels), showing a strong colocalization (white, lower panel).

(**D**) Quantification of the density of postsynaptic proteins PSD95 and Homer-1c puncta per unit length (µm) of dendrite. Red lines represent the means and dots correspond to individual cells (n = 32 and 32 fields of view respectively, from left to right; ns $p > 0.05$, Mann-Whitney test).

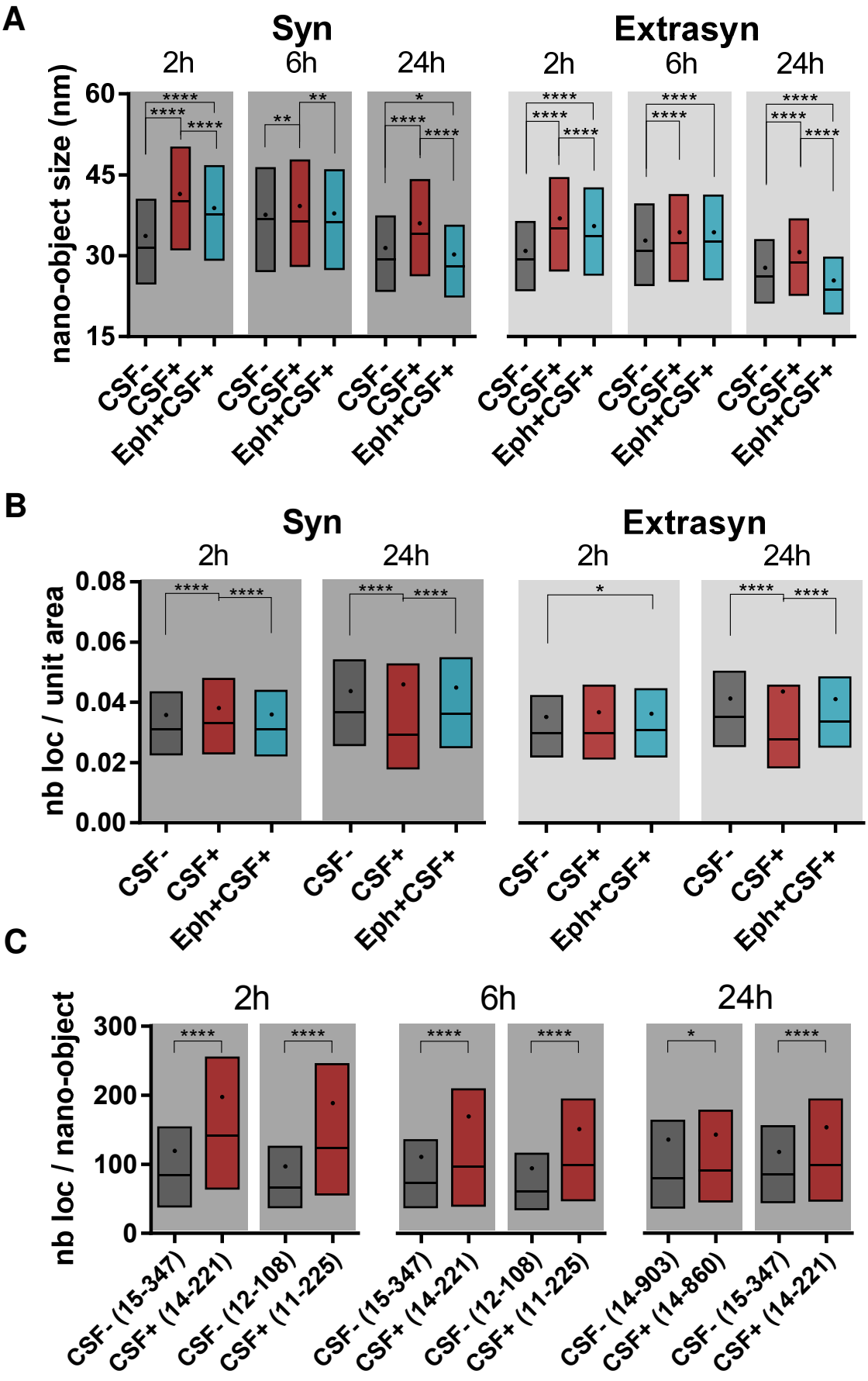
A
Syn
Extrasyn
2h
6h
24h
nano-object size (nm)
60
45
30
15
CSF-
CSF+
Eph+CSF+
B
nb loc / unit area
0.08
0.06
0.04
0.02
0.00
C
nb loc / nano-object
300
200
100
0
CSF- (15-347)
CSF+ (14-221)
CSF- (12-108)
CSF+ (11-225)
CSF- (14-903)
CSF+ (14-860)

Figure S3: NMDAR autoantibodies induce time-dependent changes in the size and receptor packing density of the NMDAR nano-objects (related to Figure 2)

Quantification of the surface NMDAR nano-object size (**A**) and localization density (number of localizations per unit nano-object area) representing the packing density of NMDARs inside nano-objects (**B**) after 2, 6 or 24 hr of incubation with the control CSF (CSF-, dark grey), the patients' CSF alone (CSF+, red) or in presence of ephrin-B2 (Eph+CSF+, cyan). The box, line and dot correspond to interquartile range (IQR, 25^{th}-75^{th} percentile), median and mean, respectively (Synaptic nano-objects size n = 3039, 4957, 4849, 5183, 5238, 4396, 2498, 3994 and 835 nano-objects respectively, from left to right; Extrasynaptic nano-objects size n = 9310, 11313, 12148, 9404, 15196, 13421, 6993, 5903 and 2001 nano-objects respectively, from left to right; Synaptic nano-objects density n = 3039, 4957, 4849, 2498, 3994 and 835 nano-objects respectively, from left to right; Extrasynaptic nano-objects size n = 9310, 11313, 12148, 6993, 5903 and 2001 nano-objects respectively, from left to right; *p < 0.05, **p < 0.01, ***p < 0.001, ****p < 0.0001, Kruskal-Wallis test).

(**C**) Inter-experiment variations in the receptor content of the NMDAR nano-objects after treatment with different batches of patients' antibodies. Quantification of the number of localizations per NMDAR nano-object after 2, 6 or 24 hr of incubation with various control (CSF-, dark grey) and patients' CSF (CSF+, red). The box, line and dot correspond to interquartile range (IQR, 25^{th}-75^{th} percentile), median and mean, respectively (n = 1045, 2033, 4560, 8810, 1733, 2390, 4279, 11899, 381, 1264, 2425, 1270 nano-objects respectively, from left to right).

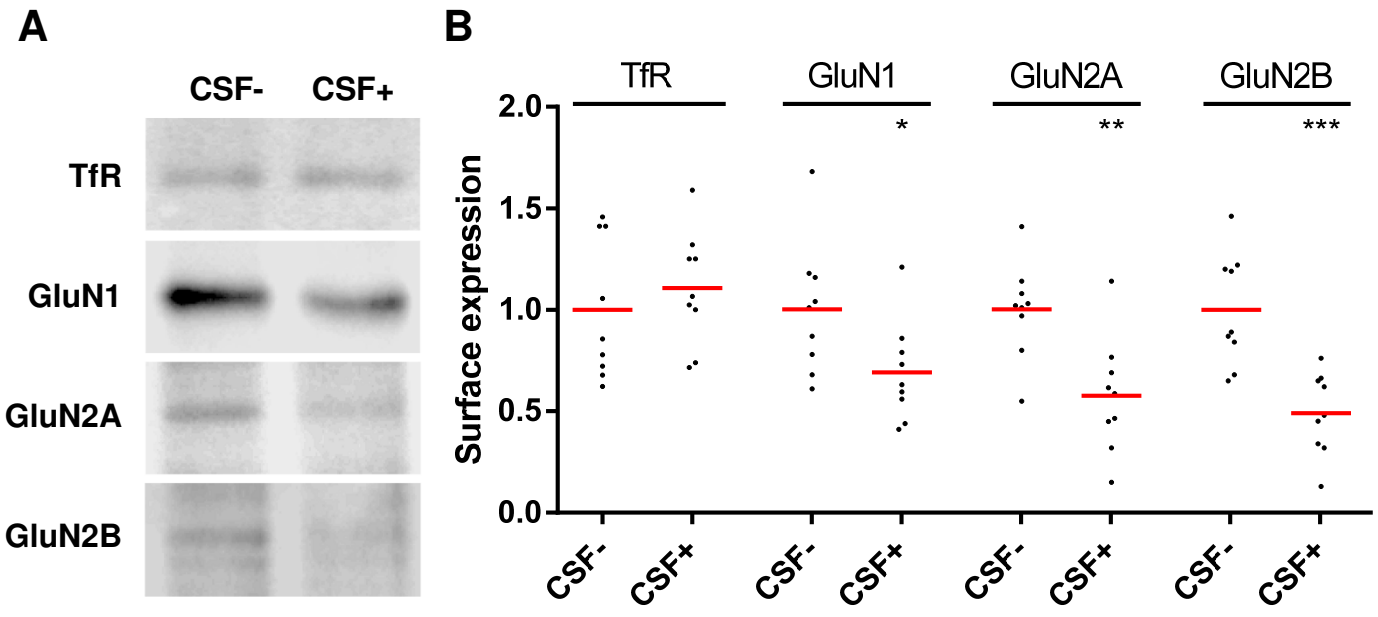

Figure S4: The protein surface levels of GluN2A- and GluN2B is reduced after 24 hr incubation with NMDAR autoantibodies (related to Figure 3)

(A) Immunoblot of biotinylated surface proteins of hippocampal neurons treated with control or patients' CSF for 24 hr. The protein bands were demonstrated using specific antibodies directed against the GluN1, GluN2A and GluN2B subunits. The transferrin receptor is used as a loading control.

(B) Quantitative densitometry analysis of the immunoblots. The data was normalized to the values of neurons treated with the control CSF. Red lines represent means and the dots correspond to individual blots (n = 9 blots for each condition; *p < 0.05, **p < 0.01, ***p < 0.001, Unpaired t-test with Welch's correction).

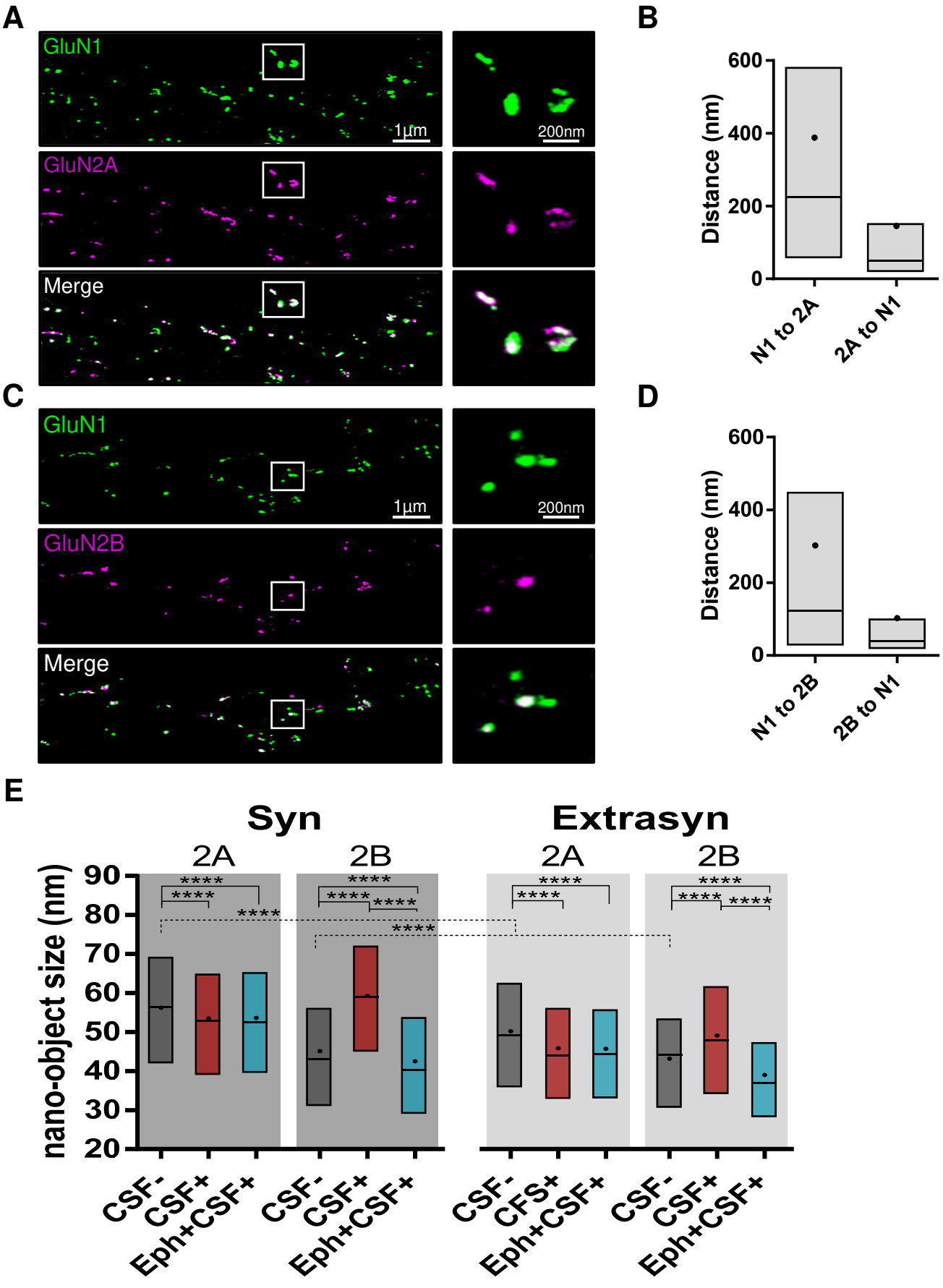
A
GluN1
1µm
200nm
GluN2A
Merge
B
Distance (nm)
600
400
200
0
N1 to 2A
2A to N1
C
GluN1
1µm
200nm
GluN2B
Merge
D
Distance (nm)
600
400
200
0
N1 to 2B
2B to N1
E
Syn
Extrasyn
2A
2B
2A
2B
nano-object size (nm)
90
80
70
60
50
40
30
20
****
CSF-
CSF+
Eph+CSF+
CFS+

Figure S5: 24 hr incubation with patients' CSF antibodies induces an increase in GluN2B-NMDAR nano-object size (related to Figure 3)

(**A, C**) Surface GluN2A and GluN2B colocalize with GluN1. Representative STORM images of GluN1 (green, upper panels) and GluN2A (**A**) or GluN2B (**C**) subunits (magenta, middle panels). Right panels display zooms of the white squared regions.

(**B, D**) Quantification of the nearest neighbor distance between the GluN1 nano-objects and the closest GluN2A/B nano-object (n = 13320 and 12722 GluN1 nano-objects respectively, from left to right), as well as the distance between the GluN2A/B nano-objects and the closest GluN1 nano-object (n = 5997 GluN2A and 7663 GluN2B nano-objects). While GluN1 is expected to be present in all NMDAR nano-objects, GluN2A and GluN2B are optional subunits that are present in a sub-population of NMDAR nano-objects. Hence, GluN1 should only partially co-localize with GluN2 whereas GluN2 should fully co-localize with GluN1, which is reflected by the much shorter distance from GluN2 to its nearest GluN1 nano-object. The box, line and dot correspond to interquartile range (IQR, 25^{th}-75^{th} percentile), median and mean, respectively.

(**E**) Quantification of the size of surface GluN2A- or GluN2B-NMDAR nano-objects after 24 hr incubation with control CSF (CSF-, dark grey), patients' CSF alone (CSF+, red) or in presence of ephrin-B2 (Eph+CSF+, cyan). The box, line and dot correspond to interquartile range (IQR, 25^{th}-75^{th} percentile), median and mean, respectively (Synaptic n = 4912, 2649, 3869, 4219, 6317 and 3162 nano-objects respectively, from left to right; Extrasynaptic n = 9312, 5213, 6395, 7938, 10086 and 7530 nano-objects respectively, from left to right; ****$p < 0.0001$, Kruskal-Wallis test for multiple comparisons and Mann-Whitney test for pair comparisons).

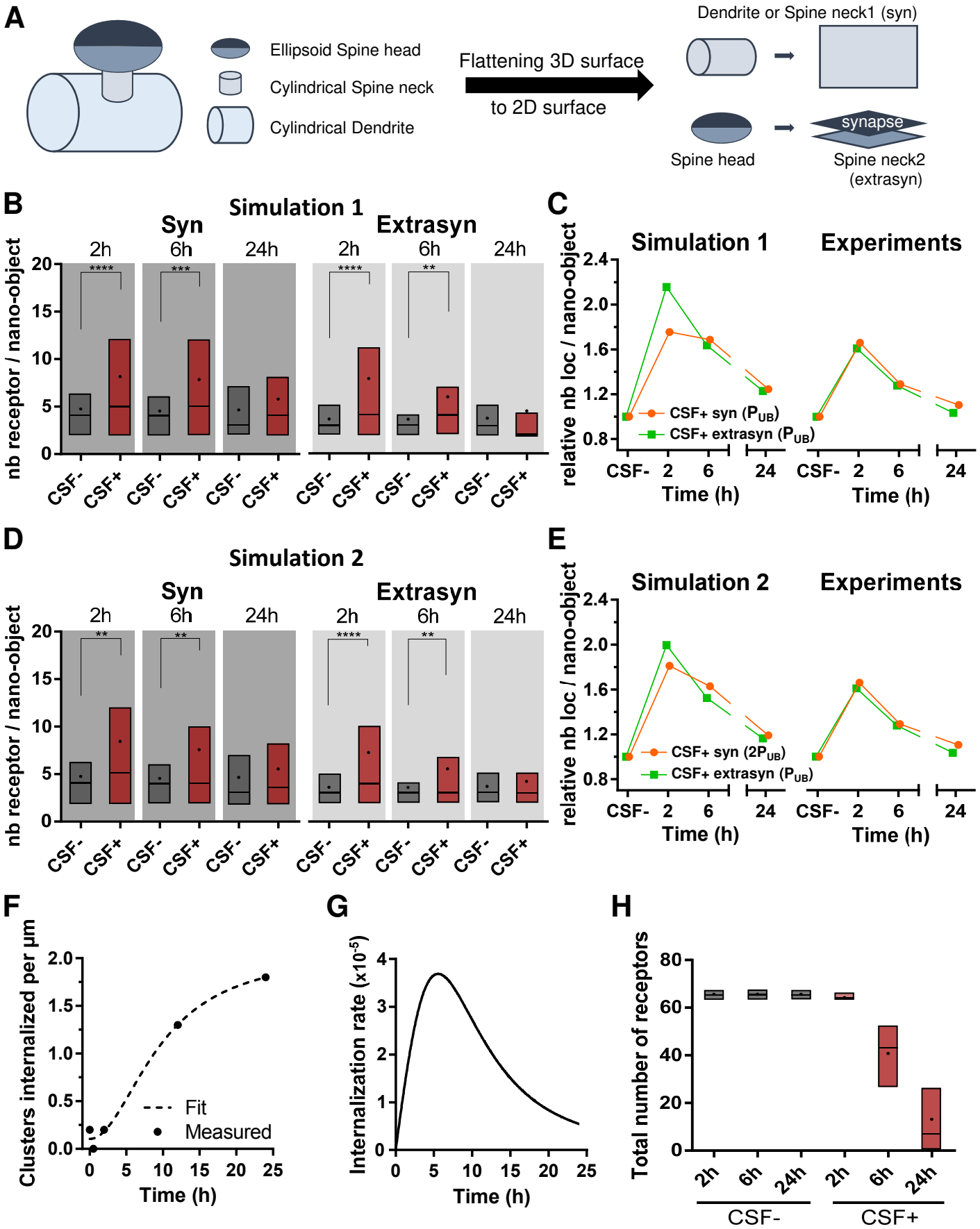
A
Ellipsoid Spine head
Cylindrical Spine neck
Cylindrical Dendrite
Flattening 3D surface
to 2D surface
Dendrite or Spine neck1 (syn)
synapse
Spine head
Spine neck2
(extrasyn)
B
Simulation 1
Syn
Extrasyn
2h
6h
24h
nb receptor / nano-object
CSF-
CSF+
C
Simulation 1
Experiments
relative nb loc / nano-object
CSF+ syn (P_UB)
CSF+ extrasyn (P_UB)
Time (h)
D
Simulation 2
E
Simulation 2
Experiments
CSF+ syn (2P_UB)
F
Clusters internalized per µm
Fit
Measured
Time (h)
G
Internalization rate (x10^-5)
H
Total number of receptors
CSF-
CSF+

Figure S6: Monte Carlo simulations suggest binding time of receptor to scaffold protein affects cluster content in synapse and extrasynapse for CSF+ (related to Figure 4)

(**A**) Schematic description of how the neuronal surface areas were generated for the simulation. Dendrite is represented by a cylinder surface, the spine consists of a cylindrical neck (spine neck1, considered extra synaptic) and an ellipsoidal spine head (bottom surface is spine neck2 considered extrasynaptic, and top surface is the synapse). Area is calculated for each of the surfaces and then flattened to a 2D surface of equivalent area.

In (**B, C**) the probability of receptor unbinding from SPR under control and antibody conditions in both extrasynapse and synapse is P_{UB}=0.167 (Synaptic n = 282, 218, 289, 158, 277 and 73 nano-objects respectively, from left to right; Extrasynaptic n = 220, 179, 222, 122, 218 and 58 nano-objects respectively, from left to right). In (**D, E**) the probability of receptor unbinding from SPR under antibody condition in extrasynapse is the same (P_{UB} =0.167), but in the synapse is $2P_{UB}$=0.333 (Synaptic n = 282, 201, 289, 141, 277 and 46 nano-objects respectively, from left to right; Extrasynaptic n = 220, 196, 222, 120, 218 and 60 nano-objects respectively, from left to right).

(**B, D**) Distribution of receptors per nano-object at 2, 6 and 24 hr time points in the synapse and extrasynapse, in both CSF- and CSF+ conditions, obtained from simulation. The box, line and dot correspond to interquartile range (IQR, 25^{th}-75^{th} percentile), median and mean, respectively, (**p < 0.01, ***p < 0.001, ****p < 0.0001, Mann-Whitney test).

(**C, E**) Comparison of the fold-change in nano-object content at different time points (2, 6 and 24 hr) relative to the corresponding CSF- values for simulations (left) and experimental data (right). Each data point is obtained by normalizing the mean of receptors per nano-object value at each time point for CSF+ with the mean of receptors per nano-object value obtained from the corresponding time points for CSF-.

(**F**) Cumulative number of internalized nano-objects per micron for CSF+ at different time points. Data points are derived from experimentally obtained number of nano-objects per micron remaining on the surface at 2, 6 and 24 hr for CSF+ (Figure 1B) and then fitted to the Logistic function y = A2 + (A1-A2)/(1 + (x/x0)^p).

(**G**) Rate of nano-object internalization derived from experimental observation. Data points are obtained by differentiating the fit representing cumulative number of internalized nano-objects per micron for CSF+ at different time points.

(**H**) Total number of receptors present on the surface of neuron at 2, 6 and 24 hr for CSF- and CSF+, obtained from simulation. The box, line and dot correspond to interquartile range (IQR, 25^{th}-75^{th} percentile), median and mean, respectively (n = 40, 40, 40, 50, 50 and 48 runs respectively, from left to right).

Table S1: List of different patient CSFs used in each experiment (related to Experimental Procedures)

Experiment	# CSF+	# CSF -
GluN1		
Confocal	11-110 & 12-053	12-266 & 13-164
STORM		
2h xp1	14-221	15-347
2h xp2	11-225	12-108
2h xp3	11-225	12-108
6h xp1	14-221	15-347
6h xp2	14-221	15-347
6h xp3	11-225	12-108
6h xp4	11-225	12-108
24h xp1	12-053	13-164
24h xp2	14-860	14-903
24h xp3	14-860	14-903
24h xp4	14-860	14-903
24h xp5	14-860	14-903
24h xp6	14-860	14-903
24h xp7	14-221	15-347
24h xp8	14-221	15-347
GluN2A-2B		
Confocal	14-221	15-347
STORM		
xp1	14-221	15-347
xp2	14-221	15-347
xp3	14-221	15-347

SUPPLEMENTAL EXPERIMENTAL PROCEDURES

Primary cultures of neurons

Briefly, primary hippocampal neurons were prepared from stage E18 embryos extracted from pregnant Wistar rats. Embryonic brains were extracted from the skull using fine forceps. Hippocampi were isolated, trypsinated in 0.20% Trypsin solution in Hanks' Balanced Salt Solution (HBSS) buffer (Sigma-Aldrich, St Louis, MO) for 15 min at 37°C, washed twice in HBSS buffer for 5min and mechanically disaggregated by pipette suction in high glucose DMEM medium (complemented with 10% Horse Serum, 10% Fetal Bovine Serum, 1% L-Glutamine, 1% Penicillin-Streptomycin and 1% Sodium Pyruvate) (Sigma-Aldrich). Neurons were plated at 120,000 cells per Corning 35 mm (P35) dishes (Sigma-Aldrich) in Neurobasal medium supplemented with B-27 Supplement (Thermo-Fisher, Waltham, MA) on poly-L-lysine-coated (Sigma-Aldrich) coverslips. Cells were maintained at 37°C, 5% CO2, 95% humidity and neurons were cultured for 16-21 days *in vitro* before use.

Animal procedures were conducted in accordance with standard ethical guidelines (European Communities Directive 86/609/EU) and approved by the local ethical committees.

CSF samples and treatments

Samples of CSF from 5 different patients with high titer of NMDAR antibodies (CSF+, determined according to previous studies, see Dalmau et al., 2008) were used on cultured neurons to determine the effects of the patients' antibodies (**Table S1**). Samples of CSF from 5 different subjects lacking antibodies that target NMDAR (CSF-) were used as controls (**Table S1**). The treatment consisted in adding 40 µl of patients' or control CSF to the cultured hippocampal neurons P35 plates containing 1 ml of Neurobasal medium supplemented with B-27 Supplement (Thermo-Fisher). At the end of the desired treatment time (depending on the experiment), cultures were washed with phosphate buffered saline (PBS). Written consent for studies was obtained from patients or from families if patients were judged unable to give consent. Studies were approved by the institutional review board of Hospital Clínic and Institut d'Investigacions Biomèdiques August Pi i Sunyer (IDIBAPS), Universitat de Barcelona.

Immunostaining for confocal microscopy

To determine the surface levels of NMDAR subunits, live neuronal cultures were incubated 1 hr at 37°C with either patients' CSF (used as an anti-GluN1 antibody, 1:200, Hospital Clínic, Barcelona), rabbit antibodies directed against surface epitopes of GluN2A (1:200, ACG-002, Alomone, Jerusalem, Israel) or GluN2B (1:200, ACG-003, Alomone). After washing with equilibrated culture medium, neurons were then incubated 30 min with either Alexa Fluor 488 goat anti-human IgG (A11013, 1:1000, Molecular Probes) or Alexa Fluor 488 goat anti-rabbit IgG (A32731, 1:1000, Molecular Probes) in equilibrated culture medium with 1% BSA for 30 min at 37°C. Cells were then fixed with PFA 4% in PBS for 10 min and then permeabilized with 0.3% v/v Triton X-100 (Sigma-Aldrich) in PBS for 10 min at room temperature, and blocked for 1 hr with 1% BSA in PBS. Cells were then incubated 1 hr at room temperature using a mouse antibody directed against PSD95 (1:200, MA1-045, Thermo-Fisher). Following the incubation with the primary antibodies, slides were washed and incubated for 1 hr at room temperature with Alexa Fluor 594 goat anti-mouse IgG

(R37121, 1:1000, Thermo-Fisher). Slides were then mounted with ProlonGold with 4′,6-Diamidino-2-phenylindole dihydrochloride (DAPI, P36935, Molecular Probes) and results scanned at 1024x1024 lateral resolution and Nyquist optimized z-sampling frequency with a confocal microscope (Zeiss LSM710) with EC-Plan NEOFLUAR CS 100x, 1.3 NA oil immersion objective. For spot analysis we performed image deconvolution using the AutoQuantX3 software (Bitplane AG, Zurich, Switzerland) followed by automatic segmentation using the spot detection algorithm from Imaris suite 7.6.4 (Bitplane). The density of spots was expressed as number of puncta per µm length of dendrite. To determine the synaptic location of GluN2 subunits, a spot co-localization algorithm between GluN2A or GluN2B and PSD95 was applied using Imaris. The same procedure was followed to compare the density of PSD95 and Homer-1c clusters. After fixation and permeabilization, cells were incubated 1 h at room temperature using a rabbit antibody directed against PSD95 (1:200, 124002, Synaptic Systems) and a guinea pig antibody against Homer-1c (1:200, 160004, Synaptic Systems). Following the incubation with the primary antibodies, slides were washed and incubated for 1 h at room temperature with Alexa Fluor 594 goat anti-rabbit IgG (R37117, 1:1000, Thermo-Fisher) and Alexa Fluor 488 goat anti-guinea pig IgG (A-11073, 1:1000, Thermo-Fisher). Slides were mounted and analyzed as described above.

Immunoblot for biotinylated cell-surface proteins

To assess the effects of patient's antibodies on cell surface levels of GluN1, GluN2A, and GluN2B NMDAR subunits, neurons were especially plated at a density of 500,000 in P35 plates and were treated with patients' or control CSF, for 24 hr. Neurons were then washed twice in cold PBS, and incubated with 1.5 $mg.ml^{-1}$ EZ Link Sulfo-NHS-LC Biotin (Thermo Fisher Scientific) in cold PBS for 30 min at 4°C. The excess of free biotin was quenched by incubating with cold PBS supplemented with 100 mM Glycine for 20 min. Neurons were then rinsed in PBS and lysated with 150 mM NaCl, 1 mM EDTA, 100 mM Tris HCl, 1% TritonX-100, 1% sodium deoxycholate, 0.1% SDS containing protease cocktail inhibitor (diluted 1:50, Sigma-Aldrich) shaking for 1 hr at 4°C. Lysates were cleared of debris by centrifugation at 13,000g for 20 min, the supernatant was collected and protein concentration measured using the bicinchoninic acid assay (PierceTM BCA Protein Assay Kit, Thermo Fisher Scientific). Equal amount of biotinylated proteins from neurons treated with either CSF (800 µg) were then incubated with avidin-linked agarose beads (PierceTM High Capacity Neutravidin Agarose, Thermo Fisher Scientific) at 4°C overnight. The beads were rinsed with 3 column volumes of PBS, and the surface fraction was eluted with 2 column volumes of SDS loading buffer. The surface fraction was then analyzed by immunoblot. For each condition, equal amounts of proteins were loaded onto 8% SDS-polyacrylamide gels and transferred to PVDF membrane. The membrane was blocked with 5% non-fat skimmed milk and incubated with the primary antibodies at 4°C overnight. The primary antibodies used for the immunoblots were: rabbit anti-GluN1 (1:1000, G8913, Sigma-Aldrich), rabbit anti-GluN2A (1:500, AGC-002, Alomone labs) or rabbit anti-GluN2B (1:500, AGC-003, Alomone labs), or mouse anti-transferrin receptors (1:2000, clone H68.4, Thermo Fisher Scientific). After incubation with primary antibodies, membranes were incubated with horseradish-peroxidase conjugated secondary antibodies (anti-rabbit IgG; 1:1000, or anti-mouse IgG; 1:10,000) for 1 hr at room temperature, and visualized with enhanced chemiluminescence (all Amersham GE Healthcare) on a LAS4000 (GE Healthcare). Protein concentrations were quantified by using scanning densitometry with Fiji ImageJ software. Surface expression of GluN1, GluN2A, and GluN2B were normalized with that of the transferrin receptor as a loading control.

STORM Imaging

Immunostaining for STORM

To determine the synaptic distribution of NMDAR subunits, after having been treated with either control or patients' CSF for 2, 6 or 24 hr, in presence or absence of ephrin-B2 (0.5µg.ml^{-1}, 50598-M08H, Sino Biological), cultured neurons were incubated live with primary antibodies in equilibrated culture medium with 1% BSA for 30 min at 37°C. Primary antibodies used for labeling before fixation for the STORM experiments were: patients' CSF (used as an anti-GluN1 antibody, 1:200, Hospital Clinic, Barcelona), rabbit antibodies anti-GluN2A (1:50, ACG-002, Alomone) or rabbit antibodies anti-GluN2B (1:50, ACG-003, Alomone). After washing with equilibrated culture medium, neurons were then incubated with the corresponding secondary donkey anti-human or anti-rabbit antibodies (1:20, Jackson ImmunoResearch) labeled with Alexa Fluor 405-Alexa Fluor 647 dye pair in equilibrated culture medium with 1% BSA for 30 min at 37°C. Cells were then fixed with PFA 4% in PBS for 10 min and then permeabilized with 0.3% v/v Triton X-100 (Sigma-Aldrich) in PBS for 10 min at room temperature, and blocked for 1 hr with 1% BSA in PBS. Followed a 1 hr incubation at room temperature with a mouse antibody anti-PSD95 (1:200, MA1-045, Thermo-Fisher) in 1% BSA in PBS and another 1 hr incubation at room temperature with a secondary donkey anti-mouse (1:20, Jackson ImmunoResearch) labelled with Cy3-Alexa Fluor 647 dye pair in 1% BSA in PBS. The same procedure was followed to visualize synaptic structure labelling Bassoon and Homer-1c. After fixation and permeabilization, cells were incubated 1 hr at room temperature using a mouse antibody directed against Bassoon (1:400, ADI-VAM-PS003, Enzo) and a guinea pig antibody against Homer-1c (1:200, 160004, Synaptic Systems). Following the incubation with the primary antibodies, slides were washed and incubated for 1 h at room temperature with the corresponding secondary donkey anti-guinea pig antibodies (1:20, Jackson ImmunoResearch) labeled with Alexa Fluor 405-Alexa Fluor 647 dye pair and a secondary donkey anti-mouse (1:20, Jackson ImmunoResearch) labelled with Cy3-Alexa Fluor 647 dye pair in equilibrated culture medium with 1% BSA for 30 min at 37°C.

For STORM imaging, the secondary antibodies were labeled in-house with different combinations of dye pairs of activator/reporter, as previously described (Bates et al., 2007). Briefly, the dyes were purchased as NHS ester derivatives: Alexa Fluor 405 Carboxylic Acid Succinimidyl Ester (Invitrogen), Cy3 mono-Reactive Dye Pack (GE HealthCare), and Alexa Fluor 647 Carboxylic Acid succinimidyl Ester (Invitrogen). Antibody labeling reactions were performed by incubating for 40 min at room temperature a mixture containing the secondary antibody, NaHCO3, and the appropriate pair of activator/reporter dyes diluted in DMSO. Purification of labeled antibodies was performed using NAP5 Columns (GE HealthCare). The dye to antibody ratio was quantified using Nanodrop and only antibodies with a composition of 3-4 Cy3 or 4.5-5 Alexa Fluor 405 and 0.8-1.2 Alexa Fluor 647 per antibody were used for imaging.

STORM Imaging

STORM combines two concepts: single molecule localization and fluorophore photoswitching. The first concept allows one to localize the position of a single fluorophore with nanometer precision. Photoswitching makes it possible to "turn off" most fluorophores into a dark state and "turn on" only a small subset of them at a time. As a result, the images of the "active" fluorophores are isolated in space and their positions can be localized with high precision. Once all the fluorophores are imaged and their positions are localized, a high-resolution image can be reconstructed from these localizations. All imaging experiments were carried out with a commercial STORM microscope system from Nikon Instruments (NSTORM). For single color imaging, 647 nm laser light was used for exciting the reporter dye (Alexa Fluor

647, Invitrogen) and switching it to the dark state, and 405 nm laser light was used for reactivating the Alexa Fluor 647 into a fluorescent state via an activator dye (Alexa Fluor 405)–facilitated manner. An imaging cycle was used in which one frame belonging to the activating light pulse (405 nm) was alternated with four frames belonging to the imaging light pulse (647 nm). Dual color imaging was performed with two sets of secondary antibodies labeled with the same reporter dye (Alexa Fluor 647) but two different activator dyes (Alexa Fluor 405 and Cy3) (Bates et al., 2007). In addition to the 405 nm laser light, an imaging cycle with 561 nm laser light as the activating light pulse was used for reactivating Alexa Fluor 647 linked to the second activator dye (Cy3).

The emitted light was collected by a 100×, 1.49 NA oil immersion objective, filtered by an emission filter (ET705/72 m), and imaged onto an electron multiplying charge coupled device (EMCCD) camera at an exposure time of 20 ms per frame.

Imaging was done using a previously described imaging buffer (Cysteamine MEA [Sigma-Aldrich, #30070-50G], Glox Solution: 0.5 $mg.ml^{-1}$ glucose oxidase, 40 $mg.ml^{-1}$ catalase [all Sigma-Aldrich], 10% Glucose in PBS) (Bates et al., 2007).

STORM Data Analysis

STORM images were analyzed and rendered as previously described (Bates et al., 2007; Huang et al., 2008b, 2008a). Briefly, peaks in single-molecule images were identified based on a threshold and fit to a simple Gaussian to determine the x and y positions. The raw STORM data consist of a list of x-y coordinates, corresponding to the localized positions of fluorophores. There is not a one-to-one relationship between the number of localizations and the number of molecules (in our case, NMDAR subunits) in STORM images mainly for three reasons: i) the antibody epitope labeling efficiency may not be 100%, ii) each antibodies can have a different number of fluorophores and, iii) each fluorophore can undergo multiple photoswitching events, resulting in multiple localizations arising from a single fluorophore.

The final images were rendered by representing each x-y position (localization) as a Gaussian with a width that corresponds to the determined localization precision (9 nm). Sample drift during acquisition was calculated and subtracted by reconstructing STORM images from subsets of frames (typically 500–1000 frames, for which drift was assumed to be small) and correlating these images to a reference frame (typically one that is reconstructed at the initial time segment).

For multicolor images, each peak was color-coded based on whether the emission was recorded immediately after 405 nm or 561 nm activation cycle. The peaks coming from a frame not belonging to the one right after an activation frame were coded as “non-specific.” A crosstalk algorithm as described previously was applied to correct for non-specific activations by the imaging laser (Dani et al., 2010). Briefly, the number of “apparent specific” activations were calculated from the frame immediately following the activation pulse and the number of “non-specific” activations from subsequent imaging frames in the imaging cycle. Assuming that the probability of “non-specific” activations is constant across all frames, we could then determine the number of “actual specific” activations by subtracting the “non-specific activation” number from the “apparent specific” activation number. We then used these numbers to statistically subtract crosstalk due to “non-specific” activations in an unbiased way as previously described (Dani et al., 2010).

Rendered images were finally processed using a previously developed algorithm (Ricci et al., 2015). Briefly, STORM data consisting in x-y localization lists were used to construct discrete localization images, such that each pixel has a

value equal to the number of localizations falling within the pixel area (pixel size = 15 nm). From the localization images, density maps were obtained by 2-dimensional convolution with a square kernel (3x3 pixels^2). A constant threshold (15 localizations) was used to digitize the density maps into binary images, such that pixels have a value of 1 where the density is larger than the threshold value and a value of 0 elsewhere. Connected components of the binary image, composed by adjacent non-zero pixels (4-connected neighbors), were sequentially singled out and analyzed. Localization coordinates within each connected component were grouped by means of a distance-based clustering algorithm. Initialization values for the number of nano-objects and the relative centroid coordinates were obtained from local maxima of the density map within the connected region, calculated by means of a peak finding routine. Localizations were associated to nano-objects based on their proximity to nano-object centroids. New nano-object centroid coordinates were iteratively calculated as the average of localization coordinates belonging to the same nano-object. The procedure was iterated until convergence of the sum of the squared distances between localizations and the associated nano-object and provided nano-object centroid positions and number of localizations per nano-object. Nano-object sizes were calculated as the SD of localization coordinates from the relative nano-object centroid.

Analyses were performed by means of custom code written in Matlab.

Monte-Carlo simulations

The dendrite was considered as a cylinder with a length of 200 nm and radius of 100 nm, which was flattened to a 2D square area of 400 nm^2. The spine was placed randomly on the dendrite which consist of a spine neck (referred as Spine neck1) represented as a cylinder and a spine head represented as an ellipsoid (**Figure S6A**). The height and radius of the neck were selected randomly from a range of 20-100 nm, which was also flattened to a rectangular 2D surface. The spine head of the spine is an ellipsoid with height, major and minor axis dimensions selected randomly from a range of 30–100 nm. Half surface area of this ellipsoid was calculated (mean value ~ .036 um^2) and compared with area of a square (~190 nm length). The total spine head surface was thus represented by two square surfaces of 190 nm length each, stacked one above the other. The top surface is the synapse, and the bottom surface belongs to extrasynapse, referred as spine neck2 (**Figure S6A**). Scaffold proteins present on the neuron surface as concentrated pockets (Nair et al., 2013) were modelled as confined regions with square geometry for simplicity (Scaffold Protein Regions, **Figure 4A**). It was observed that the fraction of the dendritic and synaptic surface area designated to the SPRs, effected the receptor dynamics under control condition. 12 SPRs of 24 nm dimension each were distributed equally over dendritic and synaptic surfaces (tuned to recapitulate receptor dynamics for control condition). The centers of 2 SPRs were separated by a minimum distance of 34 nm, again a value tuned to represent the control receptor dynamics.

Under control conditions, nano-objects were formed due to receptors binding to regions of high density scaffold proteins (represented as SPR). Fixed number of receptors were designated to each SPR providing the initial receptors per nano-object value of the dendrite and the synapse, with 1.3 times (based on experimental observation) more receptors in the synaptic SPRs. Receptors were allowed to bind to SPRs in the synapse with probability $P_B = 1$. However, in the extrasynaptic sites receptors were allowed to bind SPRs with a lower binding probability, assuming reduced presence of SPR and/or reduced NMDAR affinity for SPR (tuned to $0.6P_B$). Receptors were allowed to unbind from the SPRs with an unbinding probability $P_{UB} = 0.167$, a value that was optimized based on previous experimentally determined residence times (1-20s) of AMPA receptors inside nanodomains (Nair et al., 2013). The unbound receptors were allowed to diffuse

with a probability $P_D = 1$. Diffusion steps were drawn from a MATLAB generated normal distribution having the variance calculated from experimentally observed diffusion coefficients of NMDA receptors (median = 1 x 10^{-3} mm².s^{-1}, 25-75% = 3 x 10^{-4} - 4 x 10^{-2} mm².s^{-1}, Mikasova et al., 2012). The above mentioned probabilities along with other adjustable parameters, including receptor density (~0.2 receptors/ nm^2), number and size of SPRs (12 SPRs with 576 nm^2 of area each), and receptor diameter (5 nm) were optimized such that the receptors per nano-object remained constant over the different time points of the control simulation (**Movie S1**). In simulation 1, we considered nano-object formation whenever 2 or more receptors came into a proximity of 9 nm (distance tuned taking in consideration the approximate diameter of a receptor-antibody complex). This effect resulted in an increase of the size of existing nano-objects, and the merging and formation of new nano-objects independent of the SPRs. Receptor cross-linking also decreased the diffusion probability of any receptor out of a nano-object (value tuned to $0.05P_D$, P_D is the receptor diffusion probability under control condition.

Simulation algorithm in detail:

a) Initial distribution of the receptors on the surface

Under control conditions, nano-objects were formed due to receptors binding to regions of high density scaffold proteins (represented as SPR). At time zero, 90% of the total receptors (*nr_total* = 70) were distributed in the SPRs forming the initial nano-objects (*nr_nano-object,* number of receptors forming nano-objects) and the rest 10% was distributed randomly outside the SPR *(nr_free,* number of receptors not part of any nano-object. 20% of *nr_free* was present in the dendrite and the rest 80% present in the synapse. Fixed number of receptors (with 10% of incorporated variation) were designated to each SPR providing the initial receptors per nano-object value of the dendrite and the synapse, with 1.3 times (experimental observation) more receptors in the synaptic SPRs. We had to tune the density and distribution of the initial receptors to recapitulate receptor dynamics under control conditions. The distribution of receptors depended on the receptors per nano-object value and was calculated by

$$(Receptors\ per\ nano\text{-}object_{dend} \times no\ of\ SPR_{dend}) + (1.33 \times Receptors\ per\ nano\text{-}object_{dend} \times no\ of\ SPR_{syn}) = nr\_nano\text{-}object$$

Coordinates for the receptors were selected randomly and the minimum distance between centres of two receptors' was 2x*rad*, where *rad* is the radius of a receptor. The radius for the receptor was also tuned and was an important parameter as it effected the steric hindrance and hence their diffusion.

b) Receptor dynamics

100 ms was taken as the iteration time step (Δt). Every simulation iteration involves the following processes.

1. Internalization: The experimental data provides the number of nano-objects per micrometer remaining on the surface (nano-object density) at 2, 6 and 24 hr for CSF+ (**Figure 1B**). From the above data we could derive the number of nano-objects internalized per micron at different time points (by subtracting the maximum value from the data set) and fit it with the Logistic function (**Figure S6F**):

$$y = A2 + (A1-A2)/(1 + (x/x0)^p)$$

By differentiating the fitted function, we obtained the rate of internalization of nano-objects for every 100 ms (**Figure S6G**). The density of nano-objects assumed for the simulation is 4 times more than experimental observation (**Figure**

1B). Therefore, the rate of internalization observed experimentally, was scaled by a factor of 4 to obtain the probability of internalization:

$$4 \times \textit{Internalization rate}(t)_{experimental} \times \Delta t.$$

Every iteration was checked for internalization of nano-objects with the calculated probability. If internalization occurred, then an existing nano-object from the dendrite was randomly selected and all the receptors comprising that nano-object was made unavailable for any further processes.

2. Diffusion: Every unbound receptor was visited in each iteration and checked for diffusion with $P_D = 1\Delta t$ (all the receptors for CSF- condition; and only receptors not part of nano-object for CSF+ condition) and $P_D = 0.05\Delta t$ (Receptors part of nano-object for CSF+ condition). Diffusion steps were drawn from a MATLAB generated normal distribution having the variance calculated from experimentally observed diffusion coefficients of NMDA receptors (Mikasova et al., 2012).

Evaluating steric effect of a diffusing receptor

If a receptor *r1*, was selected to diffuse by a step $d1 = x1 + y1$, then it can only diffuse if there is no other receptor *r2* placed at an angle θ (relative to *r1*) and at a distance less than *d1*. In case there is a receptor *r2*, *r1* will diffuse only till the boundary of receptor *r2*. *r2* and *r1* are then iterated over all the receptors respectively.

3. Boundary conditions: The boundary conditions were applied to the edges of the dendrite, neck1, neck2 and synapse surfaces. Conditions were applied so that receptors have continuity of motion over these surfaces.

4. Update receptor states after diffusion: All the receptors were updated in every iteration, after diffusion. Under control condition nano-objects were formed only in the SPRs. Therefore, after diffusion receptor position was checked and if found to be present inside SPR, it was considered part of that existing nano-object. Similarly, a receptor that diffused out of SPR, was considered a free receptor. Under antibody condition, if a diffused receptor was found to be within a distance of 9 nm from a second receptor, it was considered part of existing nano-object the second receptor belonged to. In case the second receptor was a free receptor, a new nano-object was created. All nano-objects had a number assigned to them and receptors were indexed for the nano-objects they belonged to. Nano-object numbers and receptor indexes were updated if two or more nano-objects merged into one; or a new nano-object number was assigned in case a new nano-object formed. Nano-object numbers and receptor index information was required for nano-object internalization process. Lastly, it was checked, if any diffused receptor had its position in the SPR.

5. Binding and unbinding dynamics of receptors: Every receptor was visited to check for binding and unbinding events in case they were positioned inside SPRs. Synaptic receptors bound to SPR with a probability $P_B = 1x\Delta t$ and extrasynaptic receptors with $P_B = 0.6x\Delta t$ under control conditions. The synaptic receptors were considered to bind SPR with almost certainty while the binding probability for the extrasynaptic receptors was tuned to represent the control condition receptor dynamics. Both synaptic and extrasynaptic receptors unbound from the SPR with a probability $P_{UB} = (1/6)x\Delta t$ under control conditions. P_{UB} was calculated considering 6 s as the residence time constant of the NMDAR in the SPR. The time constant was tuned from a range of 1-20s of residence times of AMPAR inside nanoclusters, observed experimentally (Nair et al., 2013). In case of antibody condition, the unbinding probabilities had to be increased in a differentiated manner for the extrasynaptic ($1.5P_{UB}$) and the synaptic ($2P_{UB}$) receptors but was implemented after 1.5 hr. The receptors in this case had unbinding probabilities similar to control simulation till 1.5 hr was reached.

6. Nano-object evaluation: At the end of every time point, the nano-objects and receptors per nano-objects were recalculated, assuming any two receptors as part of a nano-object if they were separated by 15 nm (experimental resolution).

7. Data analysis: The distribution of 'Receptors per nano-object' was calculated from all the nano-objects in the synapse/extrasynapse identified from 50 simulations (~200 nano objects). The distribution of 'Total number of receptors' present on the surface was obtained by counting the total receptors (within and outside of a nano object in synapse/extrasynapse) after every simulation. In some simulations at 24 hr time point, there were 0 receptors present both in the synapse and extrasynapse. We did not include these results in the statistics which reduced the overall $N < 50$.

Videos recapitulating the simulations results were made using the image processing toolbox Dip-image for Matlab (Hendriks et al., 1999).

Results of Simulations 1 and 2

Simulation 1: To capture the receptor dynamics in the presence of patients' NMDAR antibodies, we took into account the occurrence of antibody-induced cross-linking by allowing nano-object formation whenever 2 or more receptors came into proximity decided by their radii Second, we implemented internalization of extrasynaptic nano-objects with a rate determined from the experimental data (**Figure S5F-H**). These two effects only partially recapitulated the experimentally observed changes to NMDAR nano-objects in the presence of patients' antibodies (**Figure S6B and S6C**). With this simulation, the number of NMDARs inside the nano-objects initially increased and then decreased, similar to what was observed in the experiments. However, at the 6 hr time point, there was still significant clustering of synaptic NMDARs above levels observed in the control simulation, contrary to experimental data. In addition, the extrasynaptic clustering was substantially higher than the synaptic clustering, which is opposed to the experimental results. Therefore, antibody-induced cross-linking and internalization alone could not fully capture the experimental results.

Simulation 2: Based on previous reports (Mikasova et al., 2012; Planagumà et al., 2016) and our own data showing that activation of EphB2 antagonizes the effects of the antibodies, we hypothesized that the binding of antibodies to NMDAR leads to a disruption of its interaction with EphB2 and possibly other synaptic interacting partners. We thus increased by two-fold the unbinding rate of synaptic receptors from the SPR reflecting a potential disruption of receptor-protein interactions (see Supplemantal Experimental Procedures). This modification could recapitulate better the experimental observations at the synaptic level but the amount of extrasynaptic NMDAR clustering remained inappropriately high compared with that of the synaptic NMDAR clustering (**Figure S6D and S6E**).

SUPPLEMENTAL REFERENCES

Bates, M., Huang, B., Dempsey, G.T., Zhuang, X., and Dempsey, T. (2007). Multicolor Super-Resolution Imaging with Photo-Switchable Probes Fluorescent. Science (80-.). *317*, 1749–1753.

Dalmau, J., Gleichman, A.J., Hughes, E.G., Rossi, J.E., Peng, X., Lai, M., Dessain, S.K., Rosenfeld, M.R., Balice-Gordon, R., and Lynch, D.R. (2008). Anti-NMDA-receptor encephalitis: case series and analysis of the effects of antibodies. Lancet Neurol. *7*, 1091–1098.

Dani, A., Huang, B., Bergan, J., Dulac, C., and Zhuang, X. (2010). Superresolution Imaging of Chemical Synapses in the Brain. Neuron *68*, 843–856.

Hendriks, C.L.L., van Vliet, L.J., Rieger, B., van Kempen, G.M.P., and van Ginkel, M. (1999). Dipimage: a scientific

image processing toolbox for MATLAB. Quant. Imaging Group, Fac. Appl. Sci. Delft Univ. Technol. Delft, Netherlands.

Huang, B., Wang, W., Bates, M., and Zhuang, X. (2008b). Three-Dimensional Super-Resolution Reconstruction Microscopy. 810–814.

Huang, B., Jones, S.A., Brandenburg, B., and Zhuang, X. (2008a). Whole-cell 3D STORM reveals interactions between cellular structures with nanometer-scale resolution. Nat. Methods *5*, 1047–1052.

Mikasova, L., De Rossi, P., Bouchet, D., Georges, F., Rogemond, V., Didelot, A., Meissirel, C., Honnorat, J., and Groc, L. (2012). Disrupted surface cross-talk between NMDA and Ephrin-B2 receptors in anti-NMDA encephalitis. Brain *135*, 1606–1621.

Nair, D., Hosy, E., Petersen, J.D., Constals, A., Giannone, G., Choquet, D., and Sibarita, J.-B. (2013). Super-resolution imaging reveals that AMPA receptors inside synapses are dynamically organized in nanodomains regulated by PSD95. J. Neurosci. *33*, 13204–13224.

Planagumà, J., Haselmann, H., Mannara, F., Petit-Pedrol, M., Grünewald, B., Aguilar, E., Röpke, L., Martín-García, E., Titulaer, M.J., Jercog, P., et al. (2016). Ephrin-B2 prevents N-methyl-D-aspartate receptor antibody effects on memory and neuroplasticity. Ann. Neurol. *80*, 388–400.

Ricci, M.A., Manzo, C., García-Parajo, M.F., Lakadamyali, M., and Cosma, M.P. (2015). Chromatin fibers are formed by heterogeneous groups of nucleosomes in vivo. Cell *160*, 1145–1158.